

Final Report of Research Project on Platform Integrated 60-GHz Antennas Systems

Arnaud L. Amadjikpè and John Papapolymerou

School of Electrical and Computer Engineering, Georgia Institute of Technology,
Atlanta, GA 30308

Period of Performance: 9/14/2009-9/13/2010

I. Introduction and Statement of Purpose

The next generation wireless technology for consumer handheld devices is believed to be emerging in the unlicensed broadband 60-GHz frequency spectrum, in the very near future. As defined by the IEEE 802.15.3 TG3c, the mmWave spectrum is subdivided into four 2.16 GHz wide channels that are combined with appropriate modulations schemes to provide high-throughput data transfer in the excess of 5 Gbps. This opens opportunities for multiple applications such as wireless personal area networks (WPAN), wireless HDMI, sync & go, and wireless docking station. However, the oxygen absorption at 60 GHz requires relatively high EIRP levels (up to 27 dBi indoor and 40 dBi outdoor). Assuming a reasonable 10 dBm transmitter power level in SiGe BiCMOS technology, it is clear that high gain (17 to 30 dBi) antennas (or arrays) are required to enhance the power. The choice of suitable antenna technologies is thus of great importance. Various antenna architectures with broadside and end-fire radiation are designed and implemented in this work.

Besides, the antenna performance must be characterized when it is embedded inside the handheld device to account for platform interference issues. This work examines for the first time end-fire and broadside antennas performance integrated inside wireless platform chassis. Recommendations are provided for proper mounting of 60-GHz antenna elements in platform chassis.

II. Antennas Description

In this section, different antenna architectures for 60-GHz mobile applications are presented. They are categorized in two groups: broadside radiation and end-fire radiation. An antenna system that radiates in the direction perpendicular to its geometrical orientation has a broadside radiation pattern. An end-fire antenna system radiates in the same direction as its geometrical orientation instead. Both orientations are useful for wireless platform integration at 60 GHz.

A. Broadside Radiation

A single element patch antenna and an 8-element linear dipole array are developed (Figs. 1-2). Although a single element patch has moderate gain, its quasi-omni radiation pattern, ease of fabrication and small size make it a good candidate for integration with

mobile platforms. The required EIRP level can always be reached with the use of amplifying stages or alternatively array configurations with narrow beamwidth though. The 8-element linear dipole array realizes the narrow beamwidth feature.

The rectangular patch antenna is fabricated on an 8 mil thick liquid crystalline polymer (LCP) substrate, of relative permittivity 3 and loss tangent 0.004 at 60 GHz. Owing to the thin LCP substrate and the printed patch configuration, a limited 4.5 GHz operating frequency bandwidth is achieved. The quasi-omni radiation patterns are shown in Figs. 3a-3b. The achieved peak gain at boresight is 8.5 dBi in measurements.

To improve the bandwidth performance, a horizontal dipole above a finite size ground plane is developed. To achieve both wide bandwidth and high gain, a single element dipole is elevated at a quarter-wavelength above a 1 cm² ground plane. Eight dipole elements are then arranged in a linear array to further increase the gain. A multilayer configuration combining an 8 mil LCP layer with a 20 mil RO3003 layer is utilized to elevate the dipole. These two organic materials have the same relative permittivity and are laminated using a 1mil thick LCP bondply, as shown in Fig. 4. The proposed dipole array achieves 8 GHz bandwidth and 14-17.2 dBi peak gain in measurements. Note the narrow H plane beamwidth in Fig. 5.

B. End-Fire Radiation

A single element linearly tapered slot antenna (LTSA) and printed Yagi-Uda arrays are developed (Figs. 6-7).

The LTSA is printed on an 8 mil thick LCP substrate and fed with a microstrip line magnetically coupled to a slot line. Owing to the limited bandwidth of the microstrip-to-slot transition, the LTSA is matched over only 5 GHz bandwidth. The end-fire radiation patterns are shown in Figs. 8a-8b. The achieved peak gain varies between 9.22 and 9.98 dBi in measurements.

The switched-beam printed Yagi-Uda array is capable of pointing toward two orthogonal directions depending on the state of the single-pole double-throw (SPDT) switch integrated in the antenna substrate. The GaAs HMC-SDD112 switch from Hittite is used for proof of concept. Owing to the limited bandwidth of the CPS-to-microstrip transition, the printed Yagi-Uda array is matched over only 5.3 GHz bandwidth. The end-fire radiation patterns are shown in Figs. 9a-9b. The achieved peak gain is 10 dBi/array in measurements.

C. Remarks on Antenna Measurements in Free Space

Fig. 10 shows the antenna radiation pattern setup. These measurements were performed at the NASA Glenn Research Center, by Dr. George E. Ponchak. The antennas in free space were characterized in a 60-GHz antenna characterization system that holds the iAUT fixed at the center of the coordinates system, where it acts as the transmitting antenna. The receiving antenna rotates in an arc with a radius of 52 cm around the iAUT. An Agilent Vector Network Analyzer, a V-Band low noise amplifier on the receiving port, and a pair of 1.85 mm cables are used for the measurements. The receiving antenna is a V-Band, 25 dBi standard gain horn, and a similar antenna is used for the gain measurements performed by the substitution method. A 1.85 mm coaxial to WR-15

adapter and a 1.85 mm coaxial to GPPO microstrip launcher are used for interconnects between the cables and the horn, and the iAUT, respectively. The entire system is controlled by a Labview program.

Note that the measured radiation patterns of the broadside antennas have multiple ripples that are attributed to standing waves excited along the feed lines. In fact, the microstrip used to feed the antenna elements are electrically long to isolate the GPPO connector from the antenna element, and it is well known that electrically long lines generate standing waves. The flexible LCP substrate has a slight curvature that could not be eliminated or corrected for by placing the antenna into a fixture, and this may create a tilt in the beam direction.

The GPPO connectors (part#: B010-L15-01) are available from East Coast Microwave. They require a GPPO to 1.85 mm adapter for connection to the 1.85 mm testing cables. The connectors are mounted manually to the LCP board, and it was found that the gap between the microstrip line and the GPPO connector must be minimized to avoid an abrupt transition at the microstrip input. Improper mounting of the connectors does not excite the right mode (TE_{10}), which results in anomalous return loss and antenna radiation patterns measurements.

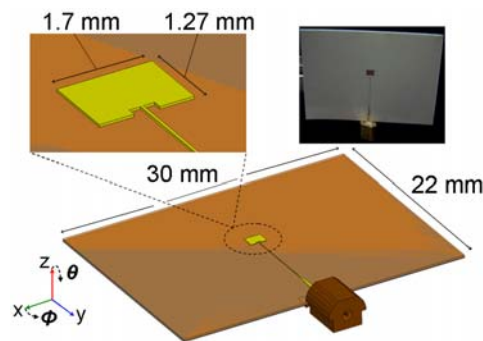


Figure 1: Rectangular patch antenna.

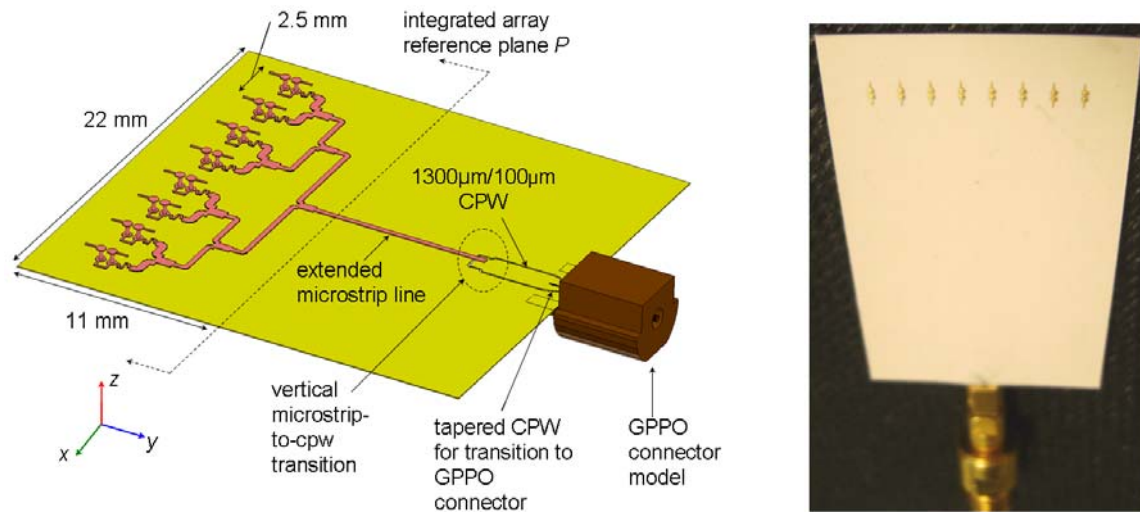


Figure 2: Proposed package-integrated 8-element dipole array.

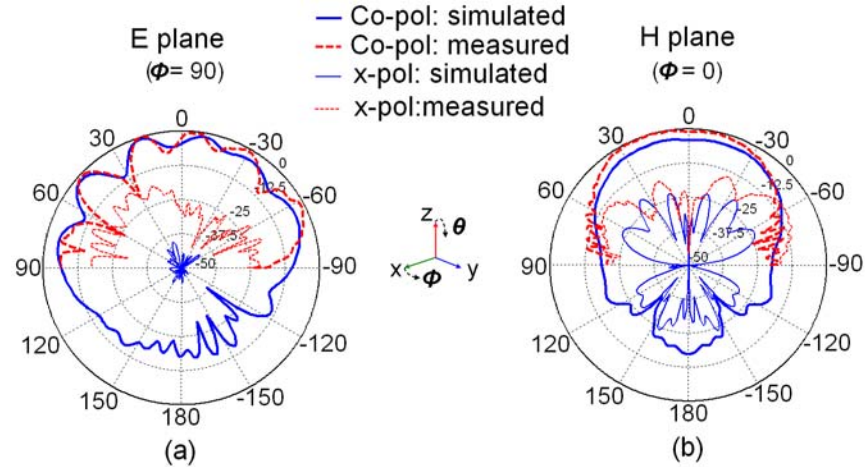


Figure 3: Simulated and measured normalized radiation pattern of the rectangular patch antenna in free space, at 60 GHz: (a) E plane; (b) H plane.

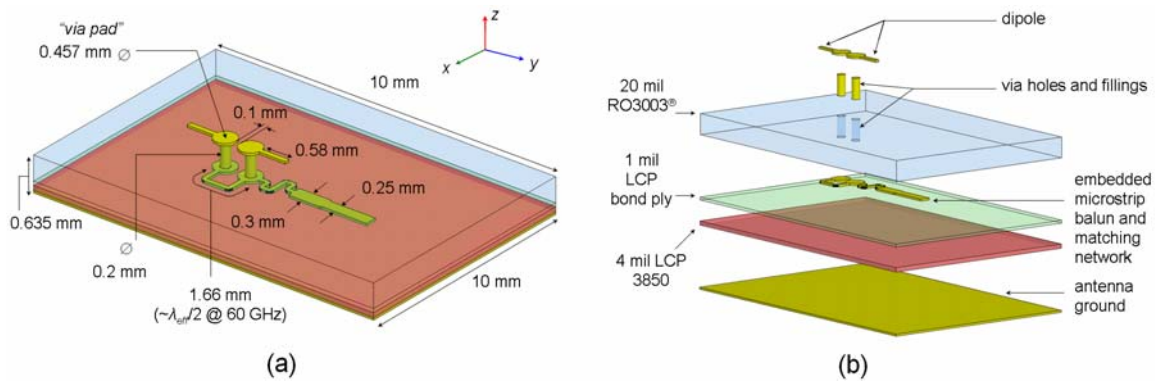


Figure 4: Schematic of the proposed package-integrated dipole: (a) 3D view; (b) Multilayer stack-up.

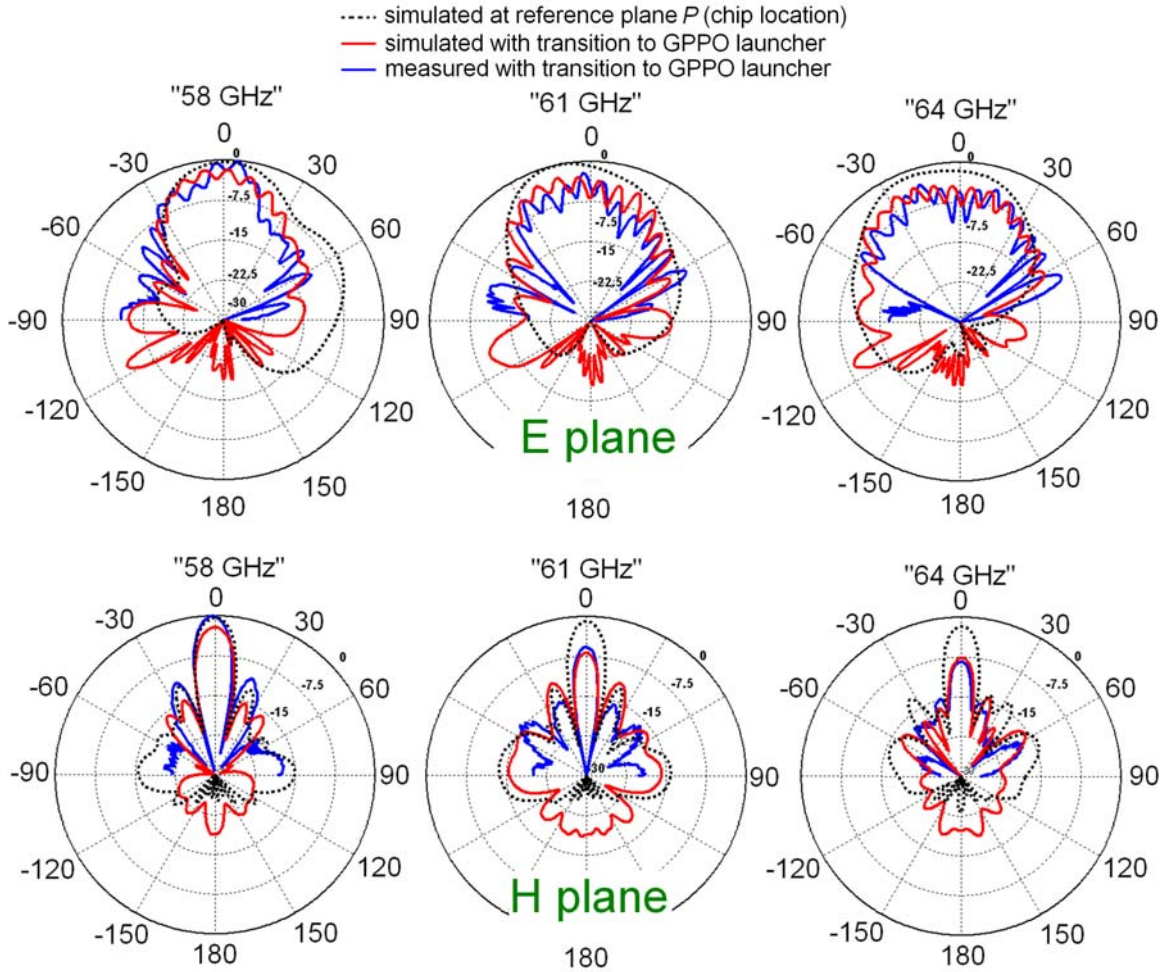


Figure 5: Simulated and measured normalized radiation pattern of the 8-element dipole array at 58, 61 and 64 GHz.

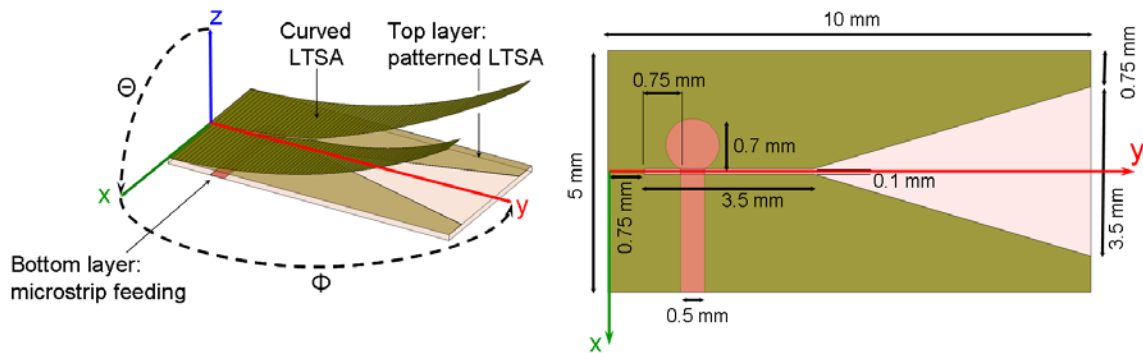


Figure 6: Linearly tapered slot antenna printed on LCP.

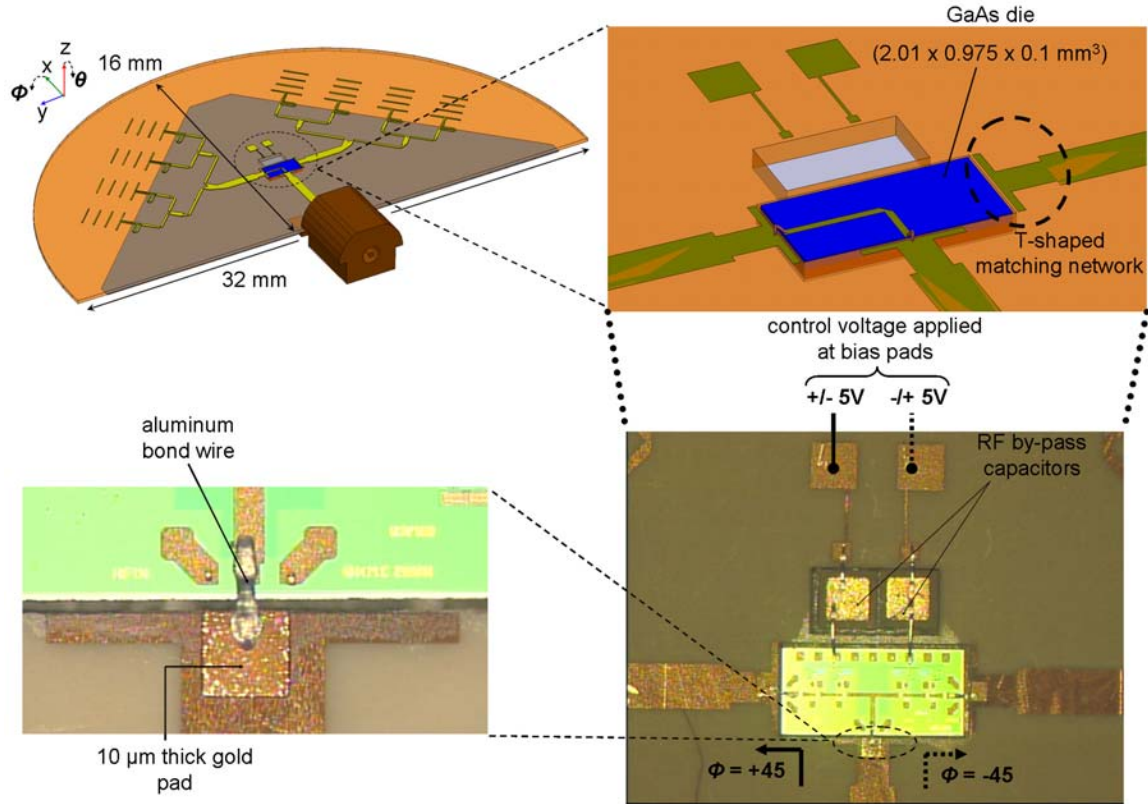


Figure 7: Schematic of the proposed switched-beam quasi-Yagi array fabricated on LCP and integrated with the HMC-SDD112 SPDT switch.

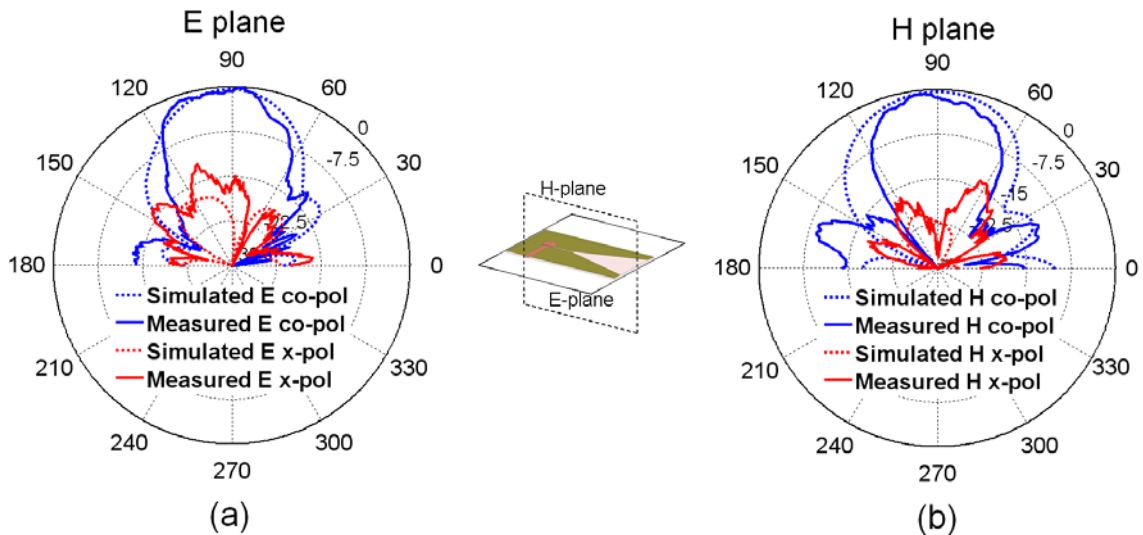


Figure 8: Simulated and measured normalized radiation pattern of the LTSA at 62 GHz: (a) E plane; (b) H plane.

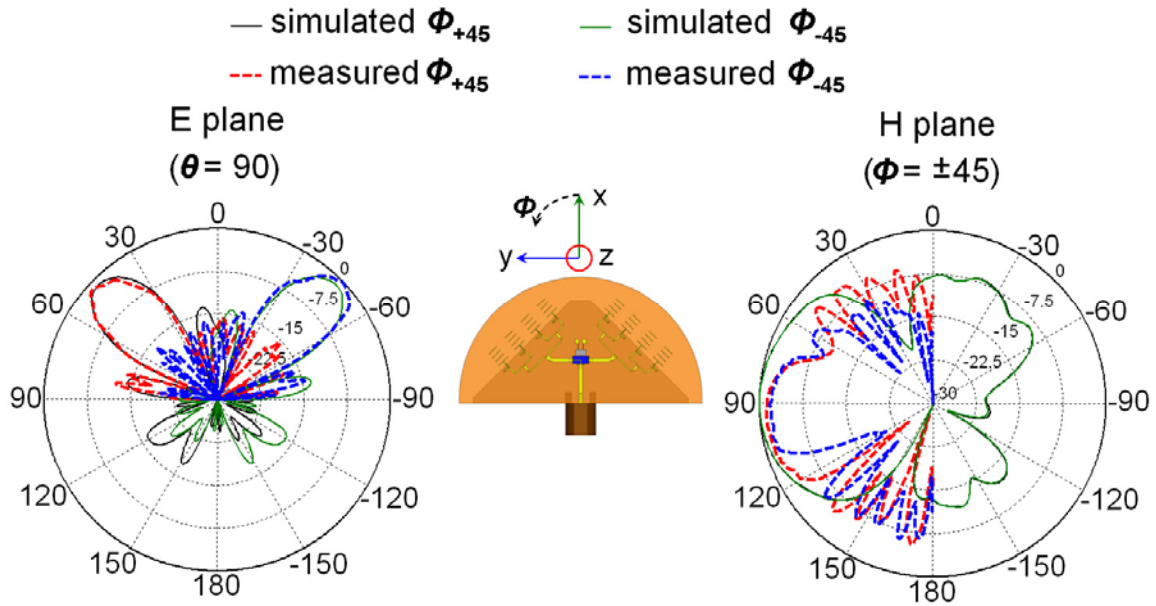


Figure 9: Simulated and measured normalized radiation pattern of the switched-beam printed Yagi-Uda array at 60 GHz: (a) E plane; (b) H plane.

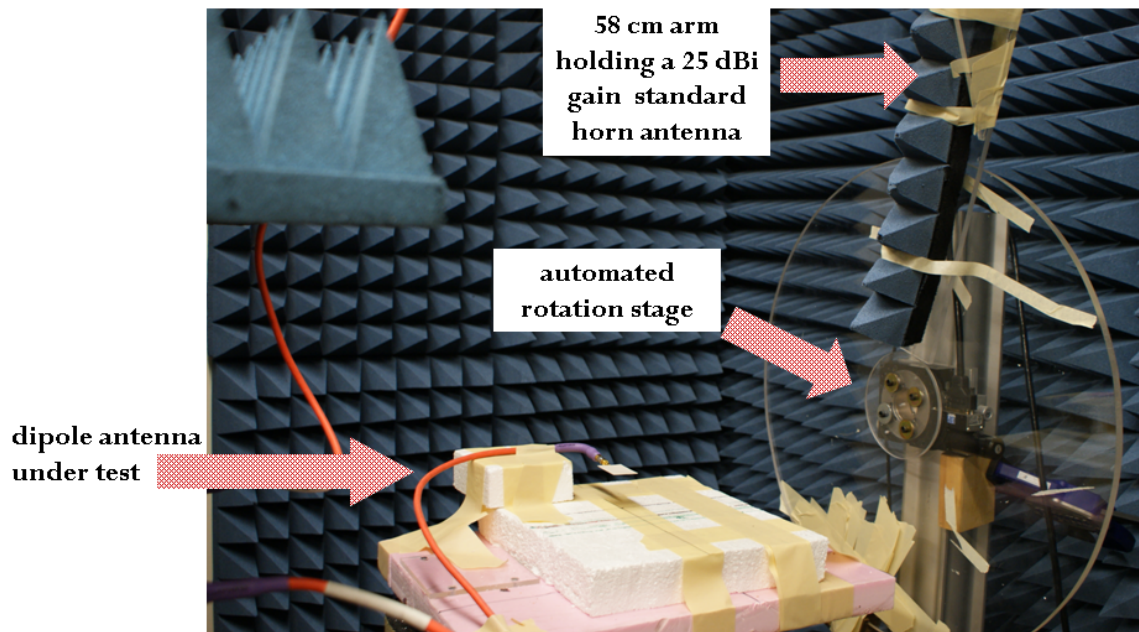


Figure 10: Antenna radiation pattern in free space measurement setup.

III. Platform Embedded Antennas

In this section, the rectangular patch and Yagi-Uda arrays are embedded inside the lid and/or the base of a laptop computer chassis to evaluate the internal performance of the antennas. A laptop chassis is chosen to perform the studies but the observations derived in this work are valid for other platforms such as smartphones, e-books, tablets, netbooks or other handheld devices.

The following section is organized as follows. The platform material is first characterized to determine its electrical properties (relative permittivity and loss tangent) at 60 GHz. Second, a CAD model for the chassis is created to simulate the entire embedded antenna system. Experiments in an anechoic chamber are carried out and compared to the simulated data.

A. Platform Material Characterization

The free space microwave beam focusing technique¹ is used to characterize the platform material at 60 GHz. The propagating energy is focused at the focal plane where the sample under test is located: the plane wave property of the focused beam allows for accurate parameters (ϵ_r , $\tan\delta$) extraction using standard Transmission or Reflection equations at a slab interface, and TRL calibration. These measurements were performed at the GTRI Materials Analysis Center (MAC). Fig. 11 depicts the measurement setup.

The extracted relative permittivity and loss tangent for a plastic laptop cover material are 3.45 and 0.025 respectively, at 60 GHz.

B. CAD Modeling

A CAD model is of interest in this study because it can be used to predict the behavior of the embedded antenna, and therefore used in the design procedure of the antenna to account and compensate for platform effects. The accuracy of the prediction depends however on the conformity of the model compared to the actual measured scenario. In other words, it is recommended to use the exact 3D model of the chassis and precisely locate the internal antenna under test (iAUT) with respect to the chassis. In this work however, the actual chassis model was not available from the manufacturer and an approximate model is generated in the Ansoft HFSS schematic modeler. Figs. 12-13 show the created and tested scenarios.

i. Lid-mounted antenna

Internal antennas are generally integrated inside the laptop lid, close to the top edge as well as side rims around and away from the LCD screen. For the location shown in Fig. 12, radiation may occur either toward $-x$, $-y$ or in the $+z$ direction. The first one represents the very familiar scenario where the antenna communicates with a spot located

¹V. V. Varadan, K. A. Jose, and V. K. Varadan, "In situ microwave characterization of nonplanar dielectric objects," *IEEE Transactions on Microwave Theory and Techniques*, vol. 48, no. 3, pp. 388-394, March 2000.

behind the laptop screen. The two other scenarios emulate an antenna communicating with wireless spots located on the front left hand of the laptop base or above the computer (a wireless spot on a ceiling for instance). Radiation toward $+x$ is here considered to be odd as it would mean that the antenna points toward the laptop user. In the simulation tool, the chassis cover material is defined as a dielectric material (with no metal particle) of relative permittivity 3.45 and loss tangent 0.025, at 60 GHz. Although plastic covers with conductive coatings are very common practices in the industry for electromagnetic interference (EMI) mitigation, this model excludes these types of covers. Indeed, preliminary measurements with a metal coated plastic cover (from a real laptop computer) show that the radiated power is attenuated by at least 40 to 50 dB at 60 GHz, which clearly prevents the use of such coatings, at least, in a small area facing the radiating element. The experimental laptop also uses a plastic cover with no metal particles. The LCD screen is defined as a glass material.

ii. Base-mounted antenna

The backside and lateral sides of the laptop base are other areas where internal antennas can be mounted. Fig. 13a shows an antenna in the front and left corner of the base that may radiate either in the $-y$ or $+z$ direction. For this particular laptop, the specific location originally contained the audio speaker which was removed, except for the $1/16$ " thick plastic obstacle and the very thin slots in the plastic. These discontinuities are included in the simulation model of the antenna placed in the surrounding laptop environment. Fig. 13b shows an antenna in the back and left side of the base, from where the internal antenna under test (iAUT) can radiate toward $-x$, $-y$ or $+z$. The laptop used for the experiments has some in-line apertures in the cover where VGA, USB and other connectors were located. These connectors were removed, and the apertures covered from the inside with small pieces of the same plastic material. In the model and the experimental laptop, a large (30 mm \times 12.5 mm) parasitic copper piece is attached 4 mm above the iAUT to investigate the proximity effects with metal obstacles.

C. Context and Physical Interpretation of Waves Propagation

The chassis integration of 60-GHz antennas can be categorized as an electrically large problem because of the very small wavelength compared to typical wireless platform sizes. For such problems, there is a common understanding that internal antenna characteristics are mainly affected by objects that obstruct the path of the rays emanating from the antenna element. The waves radiated by the internal antenna can thus be represented as rays in physical optics (PO) in which case reflections throughout the electrically large chassis surfaces are dominant effects. Although the same behavior has been observed at low frequencies with aircraft or radome mounted antennas, it is yet to be verified and demonstrated at 60-GHz with mobile platforms. Moreover, some preliminary studies conducted, as part of this project, with 60-GHz antennas in proximity of plastic cover materials showed that small size discontinuities such as thin cover edges can significantly deteriorate the antenna performance due to space wave diffraction. Because of the electrically thick platform cover, surface wave effects are also to be expected and thus to be included in the overall computation of far-fields. This behavior has been less

significant at low frequencies because the same cover edges are electrically small and thus less apparent, if not invisible at those frequencies. This emphasizes the necessity to account for the effects of small size features composing the geometry of platform environments at 60 GHz.

Fig. 14 summarizes the different distortions effects that can be generated by platforms on embedded 60-GHz antennas systems. The antenna main beam is expected to be attenuated because of the loss properties of the cover. The antenna main beam pattern is expected to be distorted because of secondary sources generated throughout the platform chassis, and due to surface waves' diffraction from edges, corners, and other structural discontinuities of the chassis. In fact, the fields radiated from the secondary sources or the diffracted fields may be in-phase or out-of-phase with the main beam, thus resulting in multiple ripples in the total radiation pattern.

D. 3dB Beamwidth Average Gain

Because of ripples that appear in the radiation patterns, it becomes tedious to determine the effective antenna gain from raw data. A higher peak gain due to constructive interference in a specific direction may not reflect the presence of a deep null in the same antenna beam. As a result, it is suggested to average the antenna gain over a 3dB beamwidth, that is, to smooth the patterns to extract the effective average antenna gain. The method proposed in this work consists in:

- smoothing rippled patterns using the MATLAB moving average method. The purpose here is to obtain data with less than 1 dB magnitude ripples in the antenna main beam. The function smooth is used to generate the smoothed data;
- a 3dB beamwidth for the smoothed patterns can then be determined, in both E and H planes; and
- the average gain G_{avg} of the AUT is finally defined as

$$G_{\text{avg}} = \frac{1}{2} \left\{ \frac{1}{N_E} \sum_{\theta_{3\text{dB}}} G_{\text{E-plane}}(\theta) + \frac{1}{N_H} \sum_{\theta_{3\text{dB}}} G_{\text{H-plane}}(\theta) \right\}$$

where N_E and N_H are the number of angular points in a 3dB beamwidth span of the E and H planes respectively, $G_{\text{E-plane}}(\theta)$ is the E plane gain at angle θ , and $G_{\text{H-plane}}(\theta)$ is the H plane gain at angle θ .

The advantage of this method is that it smoothes the gain ripples and gives an estimate of the average radiated power within the 3dB beamwidth of the antenna, hence taking into account the gain decrease due to nulls in the antenna main beam. Ideally, if we keep θ as the sweep angle, the average gain should be computed over a full 3dB solid angle (that is, the solid angle integrated over all φ angles and within $\theta_{3\text{dB}}$); but from a practical point of view, it is reasonable to limit to the E and H plane cuts.

E. Rectangular Patch Inside the Laptop Lid

Fig. 15a shows the simulated magnitude of the electric field on the surface of the laptop lid (HFSS is used to model the laptop-mounted antennas). Concentric field lines that spread out in a cylindrical fashion around the main radiator (the patch in this case)

remind of surface wave modes that are always excited in dielectrics. Excitation of surface waves on the surface and in the bulk of the chassis cover material is particularly enhanced at 60 GHz because of its large effective thickness ($1/16'' = \lambda_{\text{eff}}/2$ at 60 GHz). Surface waves usually contribute to radiation when they reach discontinuities from where reflection and/or diffraction occur. In this particular scenario, the rectangular patch is mounted 2 cm away from the lid cover edges (in the y and z directions) and the distance between the patch and the frontal cover surface is only 2 mm. Because of the 2 cm clearance distance, surface waves propagating in the cover dielectric vanish before they reach discontinuities at the lid cover edges. Therefore, there is very limited surface wave radiation and this explains why both E and H plane patterns are similar to the free space case, as shown in Figs. 15b-15c. There is a good agreement between the simulated and measured data. The H plane pattern also remains symmetric despite the large LCD glass screen behind the patch. Pattern symmetry is much more difficult to achieve at low frequencies because low frequency internal antennas require a much larger physical ground plane. Here, a 5 cm \times 5 cm wide patch ground plane is found to be large enough to hide the antenna from the LCD screen effect. The same radiation characteristics are thus expected to be observed if the patch is moved along the top or side edges of the lid. Because the fields are essentially confined in the vicinity (inside a disk of radius 4λ centered on the patch) of the patch antenna, only the lid chassis is incorporated in the simulation model. The calculated and measured power levels (averaged 3dB gain values) are 2.16 and 3.65 dBi respectively; total gain attenuations of 1.64 dB (simulation) and 2.15 dB (measurement) are extracted from the corresponding free space values. Calculated and measured attenuation levels are within 0.5 dB, which is acceptable for simulation and measurement tolerances. Here, the average gain is attenuated because part of the fields radiated from the patch is reflected at the cover interface and a more important part dissipated inside the plastic cover. Although not shown here, the cross-polarization levels were also measured and found to be better than 12 dB, same as for the standalone antenna. The limited diffraction of surface waves helps maintaining a reasonable cross-polarization level, in this specific scenario.

F. Rectangular Patch in Front of the Laptop Base

The measured radiation pattern of the base-mounted patch shows significant degradation compared to the standalone case (Fig. 17a). To better understand the behavior at this location, the patch is placed 0.5 cm from the base sidewall (closer to the base sidewall- Fig. 16b) and 2.5 cm from the inner plastic (away from the base sidewall- Fig. 16a). In the former case, the thin slots are also removed to assess their contribution (Fig. 16c). In the Fig. 17a case, a large area in the corner of the laptop base is illuminated and important surface waves are thus excited on adjacent cover surfaces. Diffracted surface waves from the sharp junction edges, corners and the thin slots radiate on one side, and reflected space waves from the inner plastic piece and surrounding cover faces interfere with the main radiated waves on the other side, which in turn significantly affect the total radiated fields (Fig. 18). In Fig. 17b, the thin slots are the essential discontinuities that create surface wave diffraction since the fields are more confined in that area. This infers that to achieve better performance from patch like antenna at this location, it first needs to be mounted as close as possible to the base sidewall to minimize

the illuminated area. Moreover, the sidewall should be free of discontinuities such as apertures or thin slots. Discontinuities in the order of a wavelength significantly diffract the excited surface waves. Although not shown here, simulations with smaller than 0.5 cm distances between the antenna and the base sidewall resulted in very consistent pattern shapes. The base-mounting scheme of Fig. 17c is therefore recommended for such antennas.

G. Printed Yagi-Uda Array in Front of the Laptop Base

Experiments and simulations performed in this case are similar to the previous ones. Thus results are briefly summarized. In this case, the full 3D radiation patterns are shown to highlight the patterns distortions. It is again observed that the antenna needs to be mounted closer the front cover surface to minimize patterns distortion.

H. Printed Yagi-Uda Array in Front of the Laptop Base

The measured radiation patterns of the base-mounted switched-beam array show some minor rippling along with a slight decrease in the average gain, in both -x and -y directions (Fig. 21). The 3dB gain values are 5.9 and 5.7 dBi respectively, which corresponds to an average 2.5 dB gain decrease in both end-fire directions, compared to the standalone antenna. These results show that end-fire antennas mounted in the back of the base have satisfactory radiation characteristics although there are minor ripples that could be avoided as explained below.

The back-left (or right) corner of the laptop base is a very complex environment where connectors or power plug-ins are usually installed. The lid proximity further makes the antenna integration problem challenging at this location. The impact on the end-fire antenna is studied here by moving the iAUT close to (0.5 cm) or far from (2.5 cm) the base sidewalls. The calculated radiation patterns turn out to significantly degrade as the antenna moves away from the base sidewalls (Fig. 22). In fact, the antenna element illuminates a larger area of the chassis when it is located 2.5 cm away from the base sidewalls. In Fig. 23b for instance, surface waves are excited not only on the surface of the base, but also on the surface of the lid; diffraction and/or reflection of these parasitic waves from the lid-base junction and also the lid and base edges and corners dramatically distort the H plane pattern (Fig. 22a). The pattern ripples result in an average 2.6 dBi gain level at boresight, that is, 5.8 dB less than the free space gain. Ripples in the patterns can thus significantly reduce the internal antenna gain, and ultimately reduce the antenna range (a 5 dB gain drop at both the transmitter and the receiver reduces the antenna range by 2/3—Friis equation). In Fig. 22c, it is observed that the main beam direction can also be significantly tilted (20° off the end-fire direction), while the gain in the plane of the end-fire antenna decreases by more than 10 dB; in this case, the plane of the end-fire antenna is just a shadow region, which leaves the antenna completely blind in its end-fire direction. The best performance of the end fire antenna is however achieved when the antenna is closer to the base sidewalls (0.5 cm antenna edge to base sidewall distance). The radiation patterns in that case are very similar to the free space case. The beam in the -x direction is even better than the -y direction because of the piece of copper mounted 4 mm above the antenna element radiating in -x: the copper piece first cancels upward

radiation in the H plane (side lobe attenuation by more than 10 dB), and second, serves as a reflector that narrows the H plane main beamwidth and increases the directivity of the antenna element in the end-fire direction. For instance, the simulated directivity of the internal antenna radiating toward -x is 14.5 dBi, compared to 12.1 dBi in free space. More generally, it can be interpreted that the top and bottom surfaces of the base chassis form a structure similar to a parallel plate waveguide (in the end-fire direction) where space waves are subject to multiple reflections, therefore resulting in a more directive beam. Note that the copper piece is electrically large ($30 \text{ mm} \times 12.5 \text{ mm}$) enough not to create a parasitic resonance at 60 GHz.

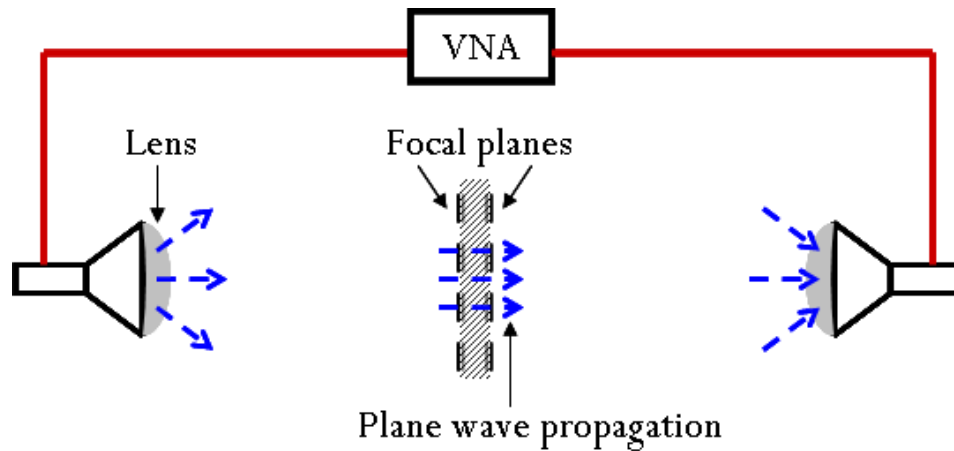


Figure 11: Platform material characterization setup using a free space microwave beam focusing technique.

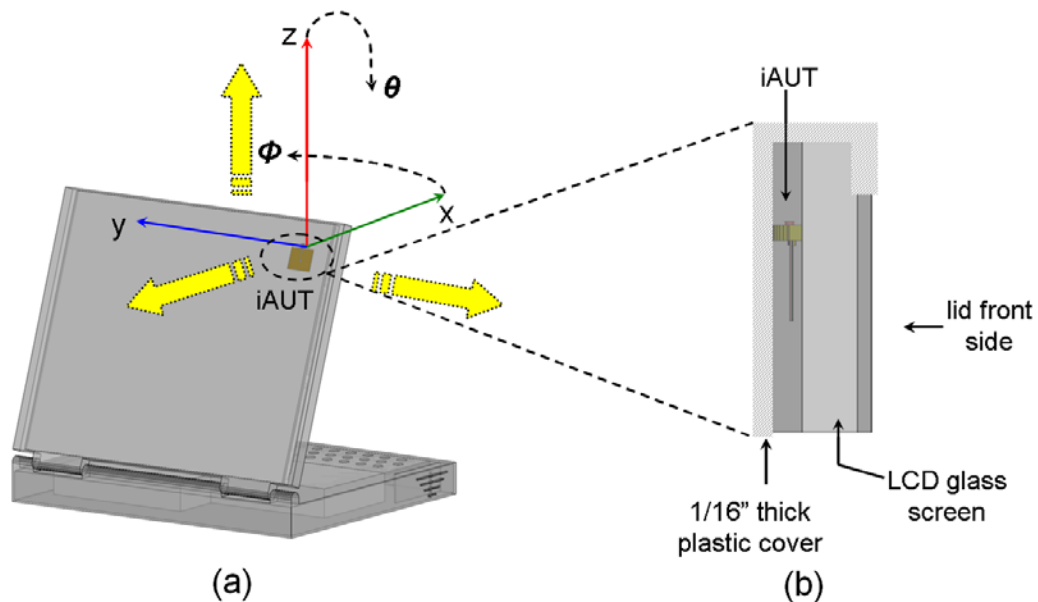


Figure 12: Antenna integration in the laptop lid: (a) back view with the center of the coordinates system aligned with the iAUT location; (b) lateral zoom on the antenna mounted behind the LCD screen. Large arrows indicate possible directions of radiation. iAUT denotes the internal antenna under test.

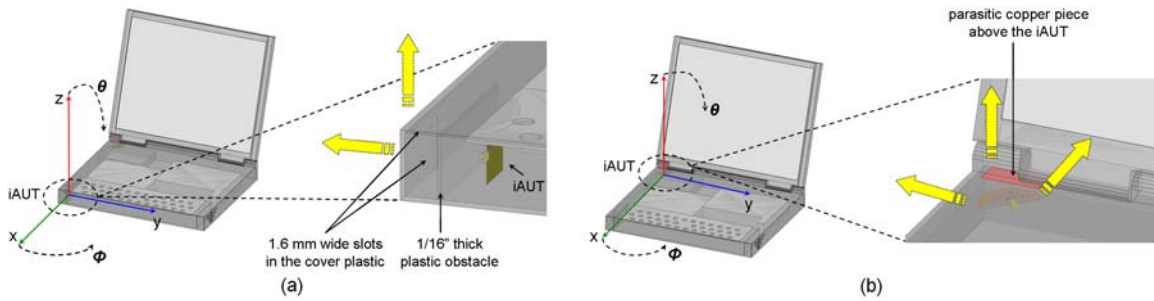


Figure 13: Antenna integration in the laptop base: (a) the antenna is mounted in the front left corner; (b) the antenna is mounted in the back left corner. In all cases, the antenna location coincides with the center of the coordinates system. Large arrows indicate possible directions of radiation.

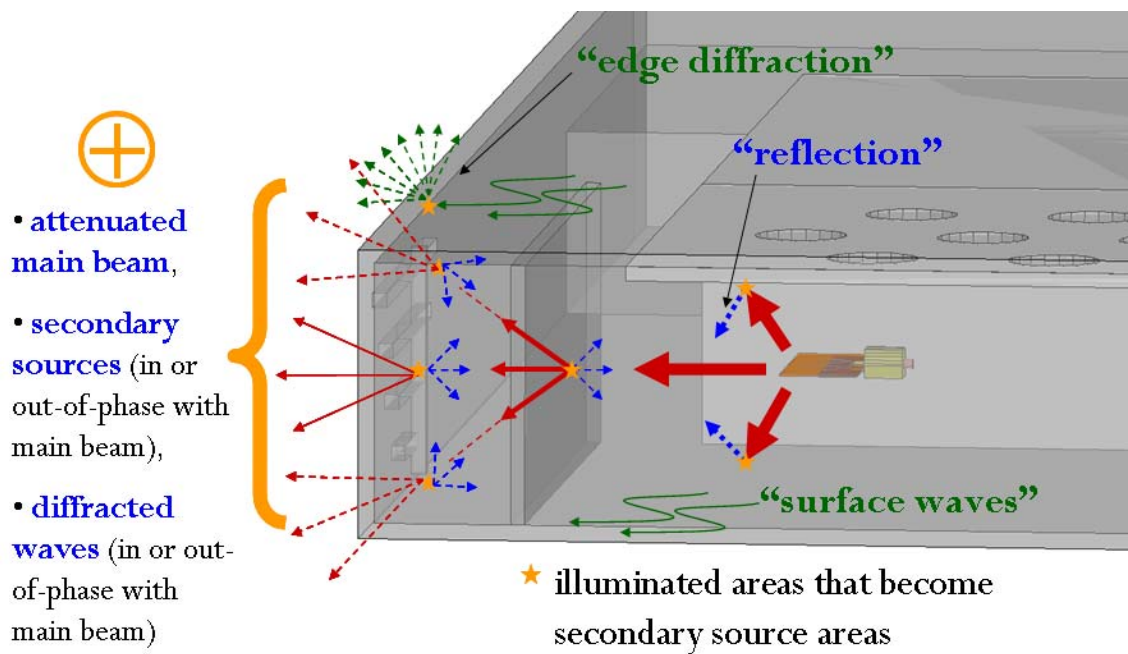


Figure 14: Physical interpretation of waves propagation inside a platform chassis at 60-GHz. A printed Yagi-Uda array is used here as an example.

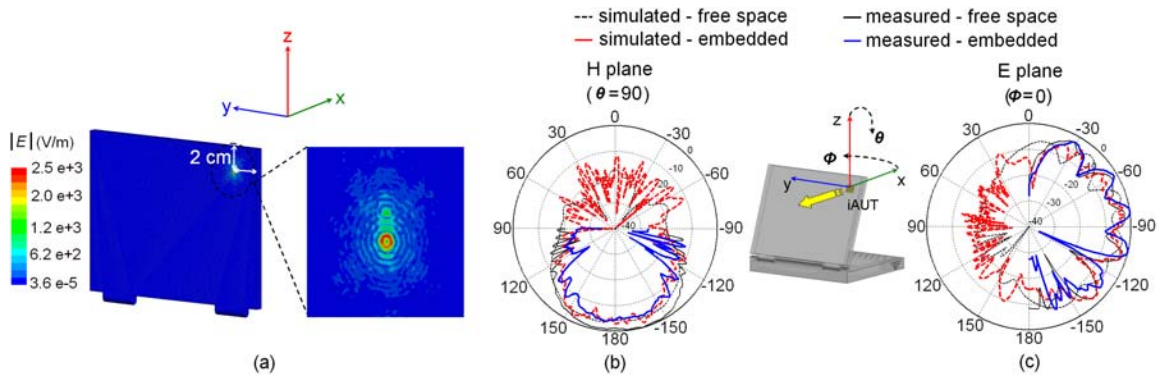


Figure 15: (a) Magnitude of electric field distribution on the surface of the laptop lid, showing surface waves excitation on the interface of the plastic cover. This is a view from the back of the laptop with a zoom into the area surrounding the patch; (b) Normalized H plane co-pol radiation pattern of the patch antenna; (c) Normalized E plane co-pol radiation pattern of the patch antenna. The antenna beam is directed toward $-x$.

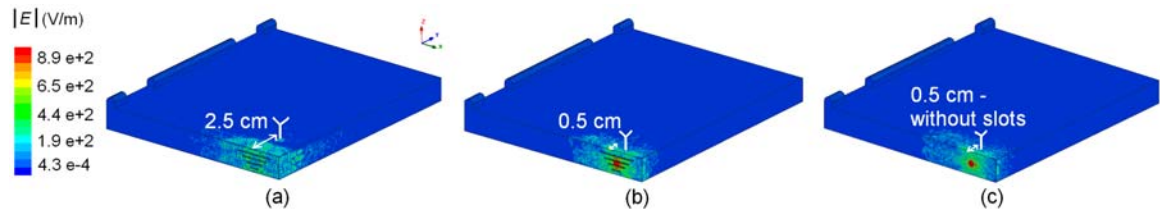


Figure 16: Magnitude of electric field distribution on the surface of the laptop base: (a) patch at 2.5 cm from the inner vertical plastic obstacle; (b) patch at 0.5 cm from the base vertical wall; (c) patch at 0.5 cm from the base vertical wall without slots in the cover. The antenna location in the coordinates system is represented by a “Y” in the plots.

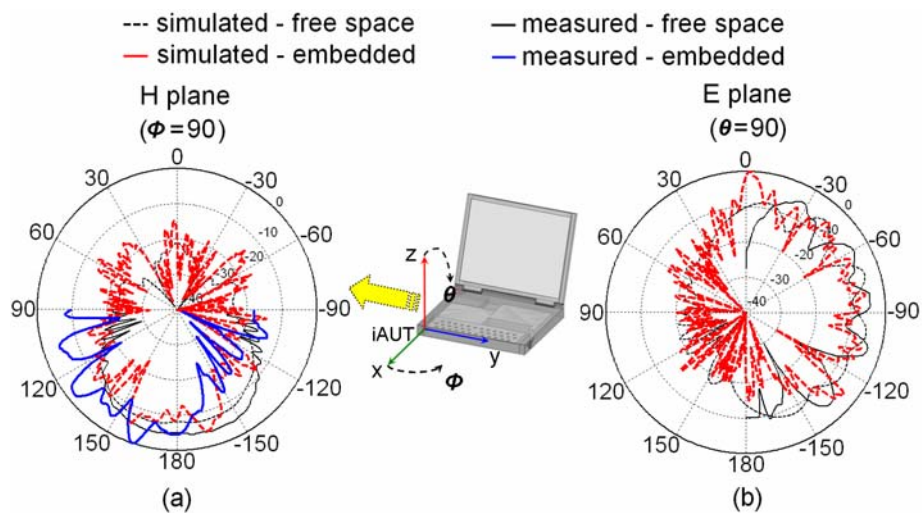


Figure 17: Simulated and measured normalized radiation pattern of the patch antenna: (a) H plane co-polarization; (b) E plane co-polarization. The antenna beam is directed toward $-y$. The E plane cut could not be measured. Standalone and integration in the front of the base are compared.

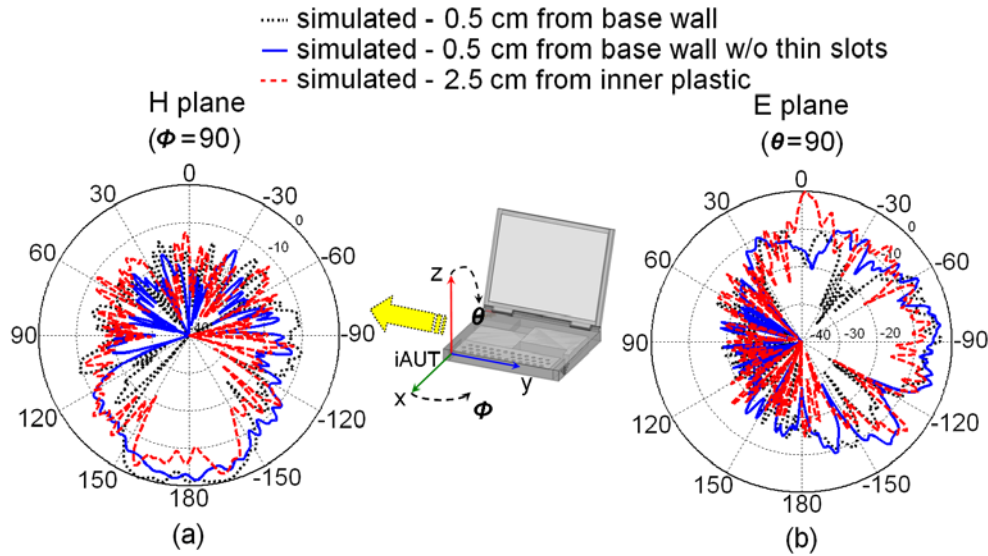


Figure 18: Simulated normalized radiation pattern of the patch antenna for different configurations: (a) H plane co-polarization; (b) E plane co-polarization. The antenna beam is directed toward $-y$.

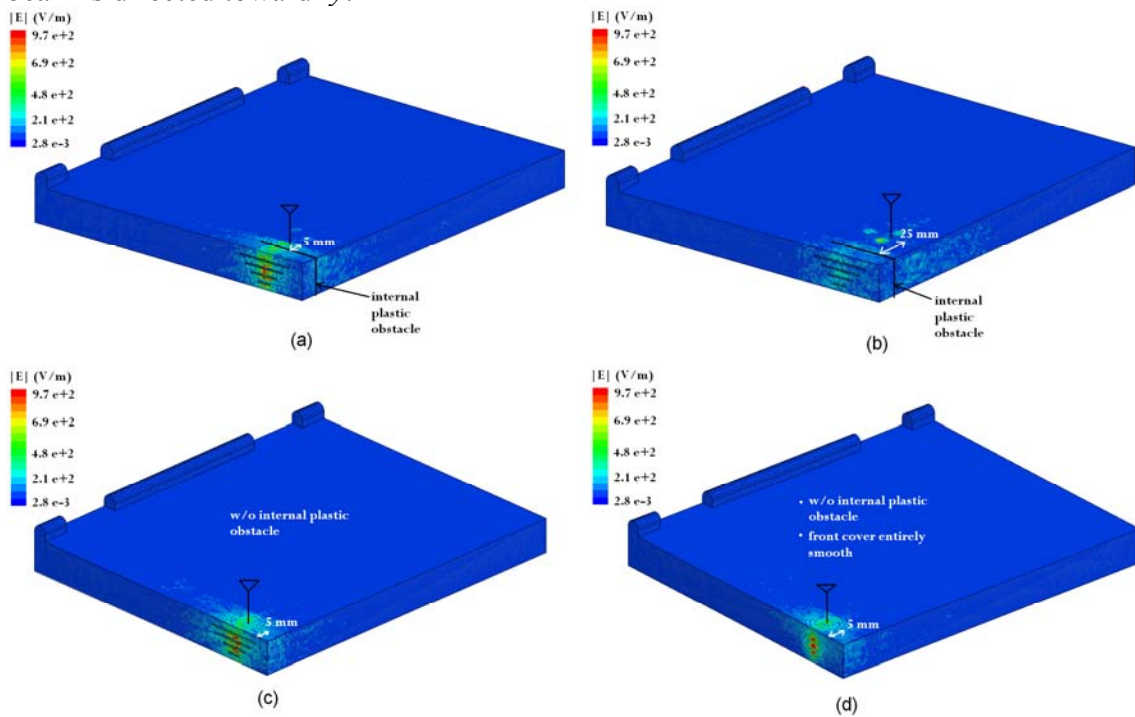


Figure 19: Magnitude of electric field distribution on the surface of the laptop base: (a) Yagi-Uda at 0.5 cm from the inner vertical plastic obstacle; (b) Yagi-Uda at 2.5 cm from the inner vertical plastic obstacle; (c) Yagi-Uda at 0.5 cm from the base vertical wall with slots in the cover; (d) Yagi-Uda at 0.5 cm from the base vertical wall without slots in the cover. The antenna location in the coordinates system is represented by a “Y” in the plots.

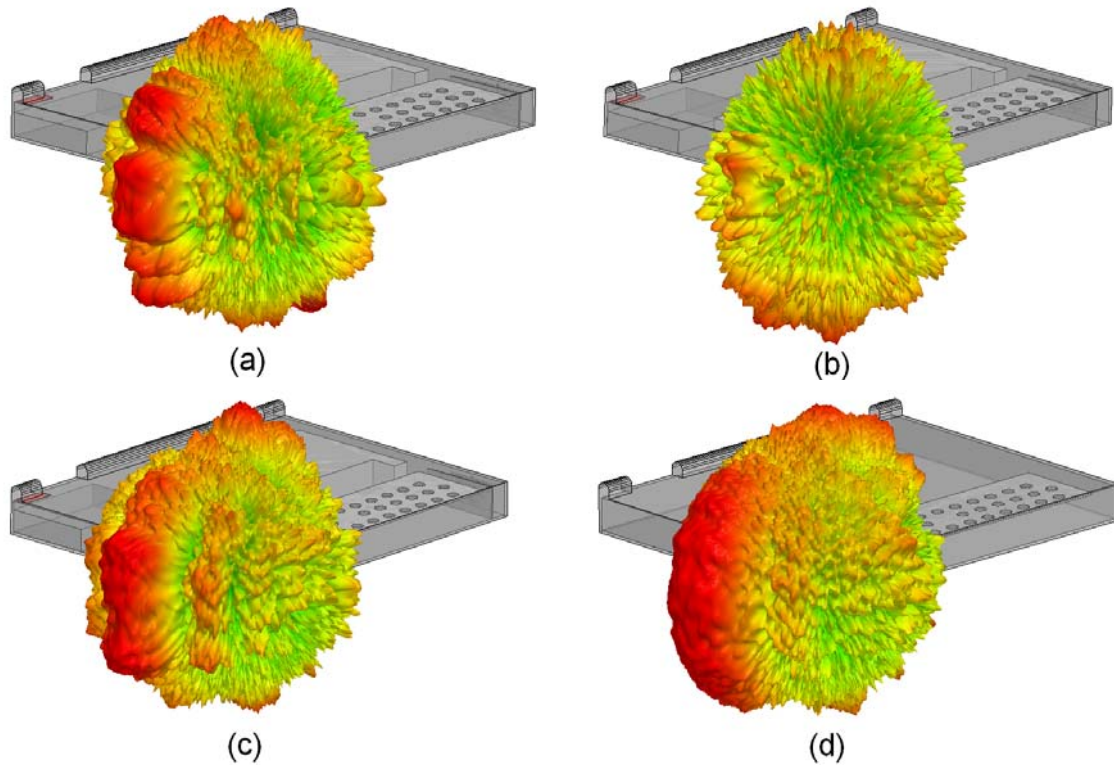


Figure 20: Simulated 3D radiation pattern of the Yagi-Uda for different configurations in front of the laptop base: (a) Yagi-Uda at 0.5 cm from the inner vertical plastic obstacle; (b) Yagi-Uda at 2.5 cm from the inner vertical plastic obstacle; (c) Yagi-Uda at 0.5 cm from the base vertical wall with slots in the cover; (d) Yagi-Uda at 0.5 cm from the base vertical wall without slots in the cover. The antenna location in the coordinates system is represented by a “Y” in the plots.

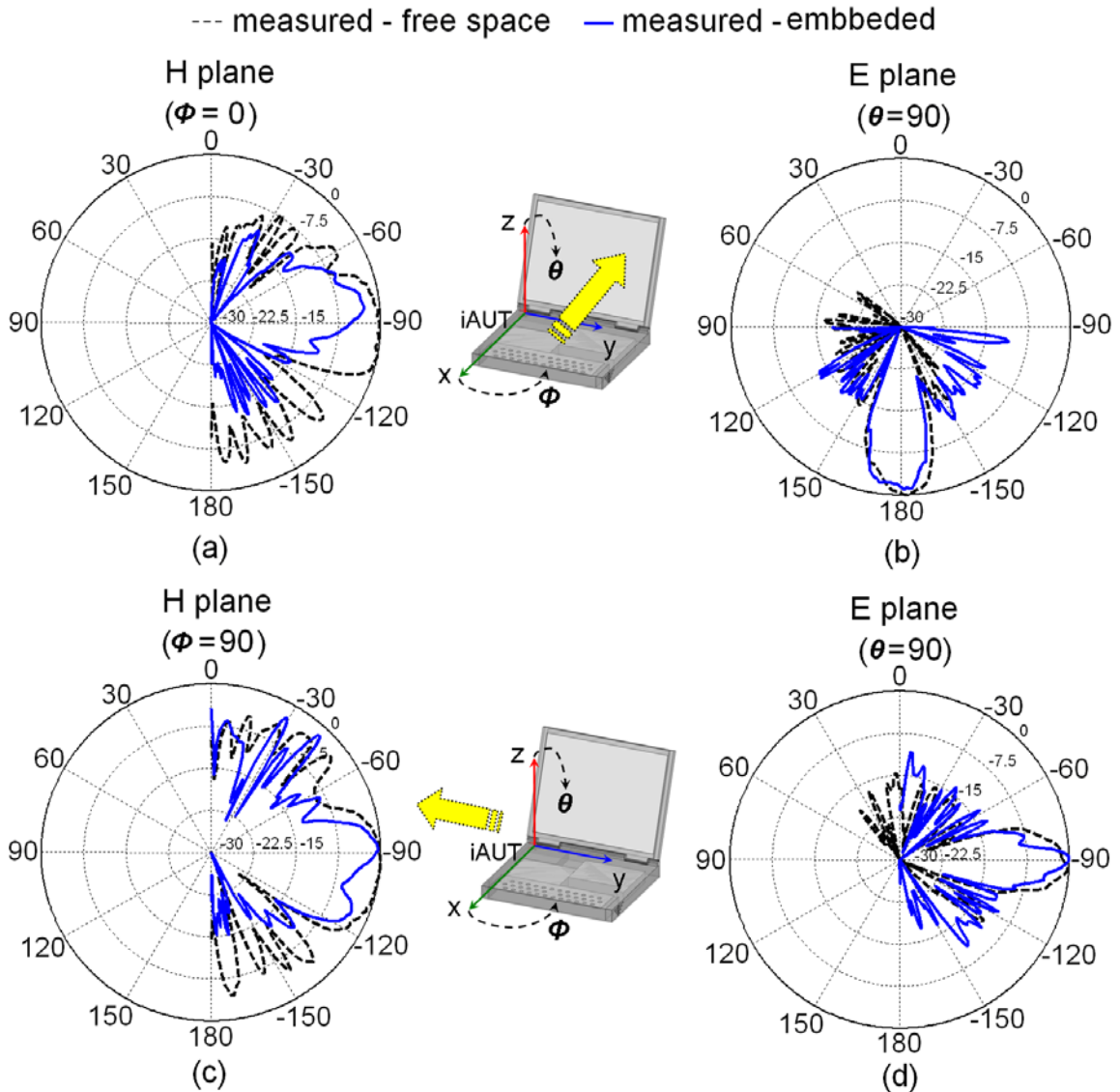


Figure 21: Measured normalized radiation pattern of the switched-beam array mounted in the back left corner of the laptop base: (a) H plane co-polarization -x; (b) E plane co-polarization -x; (c) H plane co-polarization -y; (d) E plane co-polarization -y.

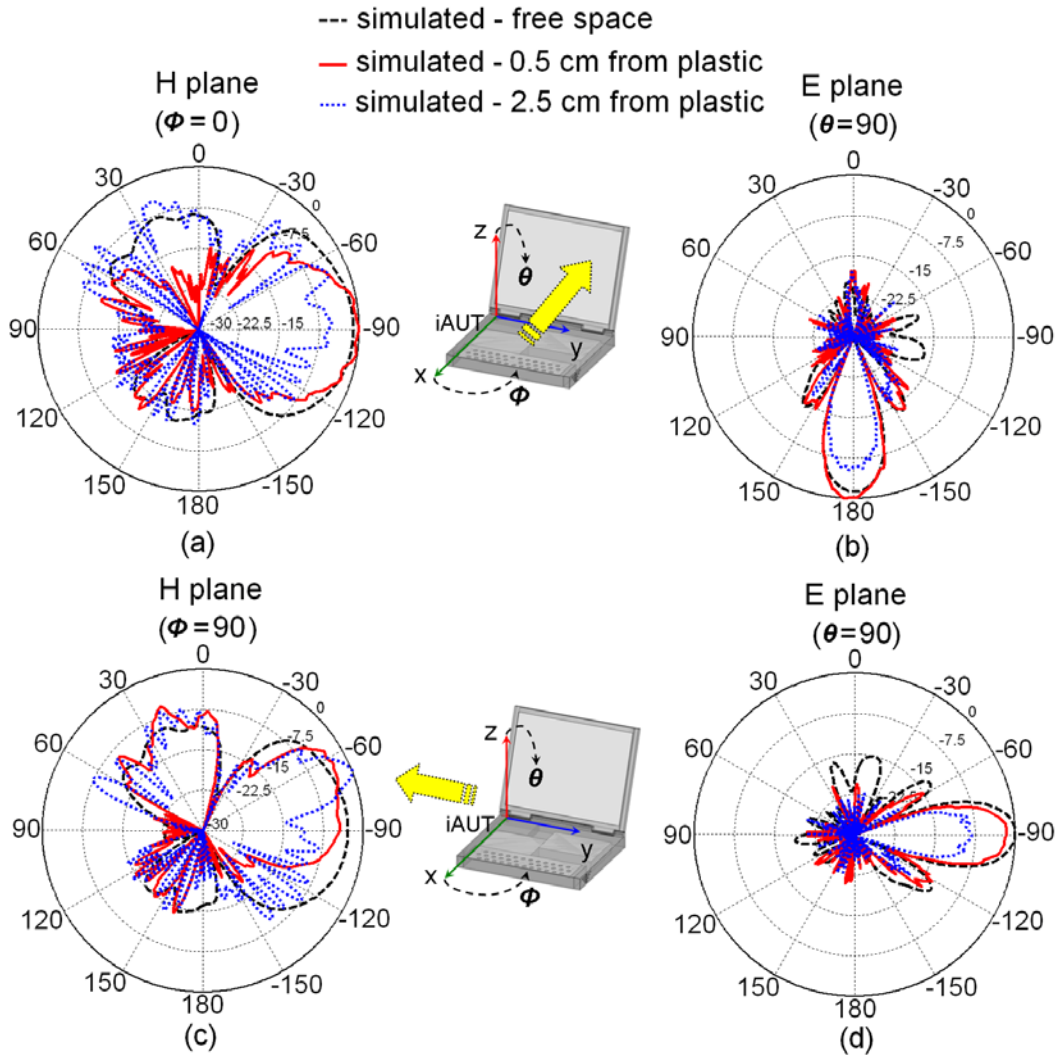


Figure 22: Simulated normalized radiation pattern of the switched-beam antenna array when located 0.5 or 2.5 cm away from the vertical plastic cover of the base: (a) H plane co-polarization -x; (b) E plane co-polarization -x; (c) H plane co-polarization -y; (d) E plane co-polarization -y.

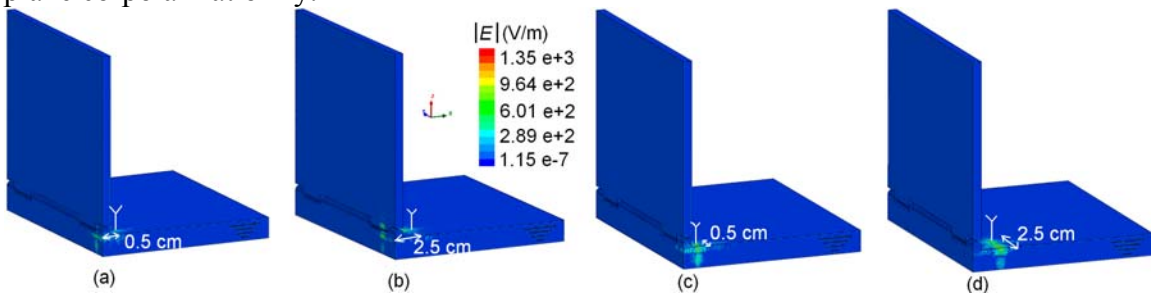


Figure 23: Magnitude of electric field distribution on the surface of the laptop lid and base: (a) switched-beam array “-x” at 0.5 cm from the base vertical wall; (b) switched-beam array “-x” at 2.5 cm from the base vertical wall; (c) switched-beam array “-y” at 0.5 cm from the base vertical wall; (d) switched-beam array “-y” at 2.5 cm from the base vertical wall. The antenna location in the coordinates system is represented by a “Y” in the plots.

IV. Results Summary and Conclusions

Platform embedded 60-GHz antenna systems are found to be extremely sensitive to the surrounding medium because of multiple factors: antenna gain attenuation, space waves reflections throughout the large chassis surfaces, and space/surface waves diffraction from structural discontinuities in the chassis. The following table summarizes the dominant factors, their causes and effects on real communication systems, and also some recommendations to mitigate the corresponding effects.

The derived results are generic and applicable to any mobile platform for embedded 60-GHz antenna systems. This study has shown that proper antenna placement along with suitable cover material choice lead to good antenna radiation performance.

	Antenna Gain Attenuation	Reflection	Diffraction
Causes	<ul style="list-style-type: none"> material dissipation: 2 to 4.5 dB depends on cover thickness and loss properties 	<ul style="list-style-type: none"> large illuminated area^a → increased number of secondary sources that radiate in or out-of-phase with the main beam fields bounce from electrically large obstacles (metal or plastic) surface waves (1/16" thick cover) reflected from λ-size discontinuities 	<ul style="list-style-type: none"> edge, corner, thin slots on cover surface space waves diffracted from these λ-size discontinuities surface waves (1/16" thick cover) diffracted from λ-size discontinuities
Effects	<ul style="list-style-type: none"> impact on link budget antenna range drop may be computed according to Friis equation 	<ul style="list-style-type: none"> multiple ripples undesired higher peak gain levels due to constructive interference → fail max. Tx EIRP level undesired nulls → signal drop beam tilt 	
Recommendations	<ul style="list-style-type: none"> avoid metal coatings in the antenna LOS account for material loss in EIRP level design 	<ul style="list-style-type: none"> mount the antenna at a distance less than 5 mm (λ) from frontal cover → minimize the illuminated area on the chassis keep cover surface smooth and free of λ-size discontinuities in the LOS use exact chassis model to predict effects and fine-tune antenna placement 	

^a The effective antenna area is limited to a small disk (radius $\approx 4\lambda$) centered at antenna element. The structure of this area dictates the overall embedded antenna performance. Away from this area, fields decay and become negligible. This means that the far-field range can be computed from the effective area and need not to be calculated using the entire platform volume.

List of Publications

A. L. Amadjikpè, D. Choudhury, G. E. Ponchak, and J. Papapolymerou, “Location specific coverage with wireless platform integrated 60-GHz antenna systems,” accepted to *IEEE Transactions on Antennas and Propagation*.

A. L. Amadjikpè, D. Choudhury, G. E. Ponchak, B. Pan, Y. Li, and J. Papapolymerou, “Proximity effects of plastic laptop covers on radiation characteristics of 60-GHz antennas,” *IEEE Antennas and Wireless Propagation Letters*, vol. 8, pp. 763-766, July 2009.

A. L. Amadjikpè, D. Choudhury, G. E. Ponchak, and J. Papapolymerou, “60-GHz Switched-Beam End-fire Antenna Module Integrated with Novel Microstrip-to-Slot Transition,” accepted to *2011 IEEE MTT-S International Microwave Symposium*.

A. L. Amadjikpè, D. Choudhury, G. E. Ponchak, and J. Papapolymerou, “60-GHz Antenna Integration in a Laptop Computer Base for WPAN Applications,” presented at *2011 IEEE MTT-S Radio and Wireless Week*, Phoenix, AZ, January 2011.

A. L. Amadjikpè, D. Choudhury, G. E. Ponchak, and J. Papapolymerou, “Highly directive package-integrated dipole arrays for low-cost 60-GHz front end modules,” *2010 IEEE MTT-S International Microwave Symposium Dig.*, pp. 348-351, Anaheim, CA, May 2010.

A. L. Amadjikpè, D. Choudhury, G. E. Ponchak, and J. Papapolymerou, “High gain quasi-Yagi planar antenna evaluation in platform material environment for 60 GHz wireless applications,” *2009 IEEE MTT-S International Microwave Symposium Dig.*, pp. 385-388, Boston, MA, June 7-12, 2009.

A. L. Amadjikpè, D. Choudhury, G. E. Ponchak, and J. Papapolymerou, “A compact conformal end fire antenna for 60 GHz wireless applications,” *2009 IEEE Antennas and Propagation Symposium Dig.*, pp. 1-4, Charleston, SC, June 1-5, 2009.

A. L. Amadjikpè, A. Vera, D. Choudhury, and J. Papapolymerou, “Study of a 60 GHz rectangular patch antenna on a exible LCP substrate for mobile applications,” *2008 IEEE Antennas and Propagation Symposium Dig.*, pp. 1-4, San Diego, CA, July 5-11, 2008.